THE JOURNAL OF PHYSICAL CHEMISTRY A

Article

pubs.acs.org/JPCA

Properties of the Only Thorium Fullerene, Th@C_{84}, Uncovered

Jakub Kaminský,*[,†] Jan Vícha,[‡] Petr Bouř,[†] and Michal Straka*[,†]

[†]Institute of Organic Chemistry and Biochemistry AS CR, v.v.i., Flemingovo náměstí 2, 166 10 Prague, Czech Republic

[‡]Center of Polymer Systems, University Institute, Tomáš Bat'a University in Zlín, Třída T. Bati, 5678, CZ-76001, Zlín, Czech Republic

Supporting Information

ABSTRACT: Only a single thorium fullerene, Th@C_{84}, has been reported to date (Akiyama, K.; et al. *J. Nucl. Radiochem. Sci.* **2002**, *3*, 151−154). Although the system was characterized by UV−vis and XANES (X-ray absorption near edge structure) spectra, its structure and properties remain unknown. In this work we used the density functional calculations to identify molecular and electronic structure of the Th@C_{84}. Series of molecular structures satisfying the ThC_{84} stoichiometric formula were studied comprising 24 IPR and 110 non-IPR Th@C_{84} isomers as well as 9 ThC_2@C_{82} IPR isomers. The lowest energy structure is Th@C_{84}-C_s(10) with the singlet ground state. Its predicted electronic absorption spectra are in agreement with the experimentally observed ones. The bonding between the cage and Th was characterized as polar covalent with Th in formal oxidation state IV. The NMR chemical shifts of Th@C_{84}-C_s(10) were predicted to guide the future experimental efforts in identification of this compound.

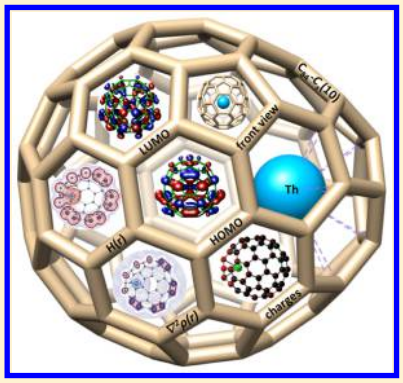

1. INTRODUCTION

Endohedral metallofullerenes (EMFs) enclose a metal atom or a cluster inside their cage. While several hundreds of transition-metal and lanthanide EMFs have been experimentally observed and characterized,[1−7] only a few actinide fullerenes are known so far, and almost nothing is known about their properties. Most of the actinide fullerene experiments have been limited to observation of their mass spectrometry signals because only a small amount of samples can be usually prepared. In this work we investigate computationally the first and so far the only experimentally reported endohedral fullerene of thorium, Th@C_{84}.[8]

The first actinide EMFs were observed in 1992 by Guo et al.,[9] who reported TOF-MS spectra of the U@C_{2n} (n = 14−36) fullerene series, such as U@C_{28} and U@C_{72}, and also some diuranium U_2@C_{2n} (n = 25−30) ones, such as U_2@C_{60} and U_2@C_{80}. Some of the monouranium compounds were later reported by Diener et al.[10] Akiyama et al. observed MS signal of An@C_{82} (An = U, Np, Am) and An@C_{84} (An = Th, Pa) series and U_2@C_{80} fullerene.[8,11−13] The experimental formation of U@C_{28} was studied.[14,15] Previously known and new diuranium fullerenes, such as U_2C_{50}, U_2C_{78}, or U_2C_{81}, were reported by means of TOF-MS signals in 2015.[16]

A number of theoretical studies of actinide fullerenes can be found. An@C_{28},[17−22] An@C_{26}, and An@C_{40} series[23,24] as well as U@C_{36}, Pu@C_{24}, and U@C_{82} have been studied theoretically.[24−27] Actinide−actinide bonding was noted by Wu and Lu in the U_2@C_{60} system[28] in 2007, and several studies followed.[29−33] We have theoretically characterized the U_2@C_{80} molecule[12] as a $^7U_2$@C_{80}-I_h(7) system where six unpaired U(5f) electrons form a double ferromagnetic bond between the enclosed uranium atoms.[33] Rather recent work investigated actinides in gold clusters[34] and versatile uranium−carbon nanostructure complexes.[35]

So far, the only experimentally characterized (besides MS spectrum) actinide EMFs are U@C_{82} and Th@C_{84}, studied by Akiyama et al.[8,11−13] For both the UV−vis/NIR and XANES, spectra were recorded. The XANES and electronic absorption spectra pointed out clearly that U@C_{82} is U@C_{82}-C_{2v}(9) system with uranium atom in oxidation state III. Theoretical calculations confirmed the experimental results and revealed a triplet ground state ^{3}U@C_{82}:9(C_{2v}).[27] Analogous M^{III}@C_{82}:9 EMFs are well known, for example, for M = Y, La, Ce, Pr.[1]

Interestingly, the results for Th@C_{84} were more difficult to interpret. Typical oxidation states of Th are IV and II. Th^{IV} could not be fully confirmed in the XANES spectra of Th@C_{84} because the corresponding absorption edge was found to be less reductive than in the reference $Th^{IV}(NO_3)_4$ material. Clear differences between the absorption spectrum of Th@C_{84} and those for previously reported isomers of Sm^{II}@C_{84} excluded a divalent Th^{II} in Th@C_{84}. Th^{III} was suspected, but Th^{III} reference material for XANES did not exist at that time. (The first Th^{III} compound has been made only recently.[36]) The ^{13}C NMR spectrum of Th@C_{84} was recorded and pointed out to a closed-shell singlet ground state of the system, but its interpretation was not possible then. It was concluded that the Th@C_{84} is probably a Th^{IV}@C_{84} system.

Notably, an M^{IV}@C_{84}-type EMF does not have any experimental precedence. Monometallic M@C_{84} compounds

Received: January 12, 2017
Revised: March 24, 2017
Published: April 4, 2017

DOI: 10.1021/acs.jpca.7b00346
J. Phys. Chem. A 2017, 121, 3128−3135

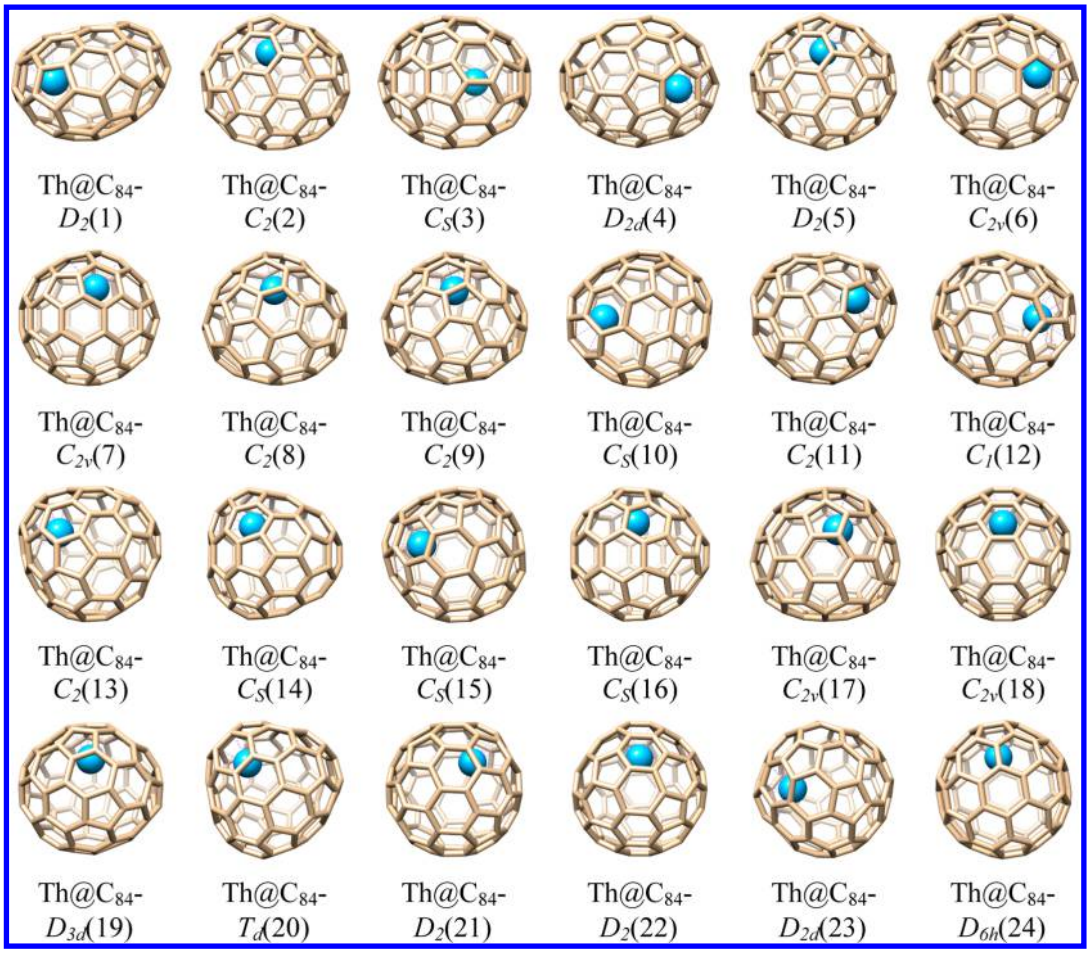

Figure 1. Structures of $Th@C_{84}$ IPR isomers optimized at the PBE0/def2-TZVPP/Th-ECP level. The Cartesian coordinates are listed in the SI.

reported up to date contain divalent metal, for example, $Sm@C_{84}$ or $Ca@C_{84}$.[1] Hence $Th@C_{84}$ presents an interesting system worth further investigation.

The aim of this work was to identify the geometry of the global minimum of $Th@C_{84}$, its electronic structure, and the character of bonding between the cage and Th atom. The UV−vis and NMR spectra of the lowest energy isomer found, $Th@C_{84}$-$C_s(10)$, were calculated to guide the future experimental efforts in identification of this metallofullerene.

2. METHODS

2.1. Structure Optimizations. The DFT calculations were performed using the Turbomole 6.3.1[37] and Gaussian 09, revision D.01,[38] program packages. Initial geometries of 24 isomers of C_{84} were taken from ref 39. The geometries of 110 non-IPR isomers with two fused pentagons were produced by the Fullerene program.[40,41] Structures were optimized at two different computational levels using either the PBE0 hybrid functional[42] with the Ahlrich's-type def2-TZVPP basis set,[43,44] which includes Stuttgart 30-valence electron pseudopotential on the Th atom[45] (PBE0/def2-TZVPP/Th-ECP level), or computationally cheaper BP86 functional,[45] with def-SVP basis set (BP86/def-SVP/Th-ECP level).[43,46,47] Different positions of Th atom inside the cage were used in starting structures to systematically explore the internal space of the fullerene. The symmetry was not maintained during optimizations to ensure the global minima for given cage. Only energetically most favorable optimized geometries are discussed in the text. Minima were confirmed by calculations of the harmonic frequencies. The electronic ground state was checked by calculations of the lowest-energy triplet state; in all cases the singlet was found to be more stable. We note that the empty-cage isomer C_{84}-$C_s(10)$ is a first-order saddle point,[48] but we kept this structure for comparison of energetics.

2.2. Bonding Analysis. Natural population analysis (NPA) as implemented in the Natural Bond Orbital[49,50] module in Gaussian 09 was employed. Molecular orbitals were plotted using the VMD software.[51] The NPA analysis and canonical orbitals were calculated at the BP86/def-SVP level. The electron density was analyzed within the context of the Quantum Theory of Atoms in Molecules (QTAIM)[52] by AIMAll suite of programs.[53] For proper treating the thorium atom in QTAIM analysis, auxiliary basis functions were added to the wave function of the molecule.[53]

2.3. Electronic Excitations. Electronic absorption spectra (vertical excitation energies and absorption intensities) were calculated using the time-dependent DFT (TD-DFT), as implemented in the Gaussian 09.[3] We used the B3LYP functional with 6-31G* basis set on carbons.[54−58] The basis set for Th with corresponding ECP[45] implemented under SDD name in Gaussian 09 code[38] was used.

The spectra were obtained from the intensities by a convolution with a Lorentzian function, using the full width at half-height of 0.05 eV.

2.4. NMR Chemical Shifts. We have previously shown that molecular properties, such as NMR chemical shifts, IR, and

DOI: 10.1021/acs.jpca.7b00346
J. Phys. Chem. A 2017, 121, 3128−3135

Raman spectra of large nanocarbon structures, can be successfully predicted theoretically.[59−64] Relativistic calculations of NMR properties were carried out using the ADF program.[65−67] The Spin−orbit Zeroth-Order Regular Approximation (SO-ZORA) as well as the spin-free scalar ZORA approach[68−70] were compared in the calculations of the ^{13}C nuclear magnetic shielding constants. Adapted PBE0 functional[4] with 40% of Hartree−Fock exact-exchange admixture, referred to as PBE40 through the manuscript, was used. The higher amount of the exact-exchange admixture led to good results in previous studies of transition-metal and actinide compounds,[71−74] admittedly due to some error cancellations.[71,75,76] Two Slater orbital basis sets, TZP and TZ2P, were used.[77,78] Calculated isotropic nuclear shieldings (σ) were converted to chemical shift (δ) using tetramethylsilane (TMS) as the reference and C_{60} as the secondary reference, according to formula

$$\delta_i = \sigma(C_{60}) - \sigma_i + \delta(C_{60}, \mathrm{TMS}) \quad (1)$$

where δ_i is the signal at a C_{84} carbon and $\delta(C_{60},\mathrm{TMS}) = 143.15$ ppm is experimental ^{13}C chemical shift of C_{60} versus TMS reference, taken as the secondary standard.[79,80]

3. RESULTS

3.1. Search for the Most Stable Isomer of ThC_{84}. The initial structures were based on 24 IPR (IPR = isolated pentagon rule) isomers of C_{84},[81] the 110 non-IPR cages with two joint pentagons, and 9 $ThC_2@C_{82}$ structures derived from IPR isomers of C_{82}. The structures of the 24 IPR isomers of C_{84} cage and their relative energies are shown in Figure S1 in the Supporting Information (SI). The stability of the empty C_{84} IPR cages is in agreement with previous studies.[39,48] The lowest isomers are C_{84}-D_{2d}(23) and C_{84}-D_2(22), while the highest energy isomer, C_{84}-D_2(1), lies ∼210 kJ/mol higher. The C_{84}-C_s(10) lies 123 kJ/mol above the lowest minimum at the PBE0/def2-TZVPP level.

Minimized structures of $Th@C_{84}$ IPR isomers are shown in Figure 1. Their relative stabilities are plotted in Figure 2 and compared with relative stabilities of the empty C_{84} IPR cages. The BP86/SVP/Th-ECP results are rather similar to those obtained at the more accurate but computationally more demanding PBE0/def2-TZVPP/Th-ECP level.

The relative stability of $Th@C_{84}$ IPR isomers is substantially different from that of the empty C_{84} IPR cages (Figure 2). This is a generally known feature caused by differential encapsulation energies corresponding to hypothetical reaction Th + C_{84} = $Th@C_{84}$; see the dotted line in Figure 2. The lowest energy IPR isomer of $Th@C_{84}$ derives from the C_{84}-C_S(10) cage. $Th@C_{84}$-C_S(10) also has the largest encapsulation energy, −737 kJ/mol. Another five $Th@C_{84}$ isomers lie within the 10 kcal/mol (42 kJ/mol) energy limit from the $Th@C_{84}$-C_S(10) lowest minimum: $Th@C_{84}$-C_{2v}(6), $Th@C_{84}$-C_2(11), $Th@C_{84}$-C_1(12), $Th@C_{84}$-C_2(13), and $Th@C_{84}$-C_S(15). They are all singlet in the ground state. The $Th@C_{84}$-D_{2d}(23) and $Th@C_{84}$-D_2(22) derived from the most stable empty-cage IPR isomers are high on the relative energy scale due to the smaller Th encapsulation energy; see Figure 2.

The HOMO−LUMO gap usually serves as a helpful indicator of stability of fullerenes. The low-energy isomers of $Th@C_{84}$ have HOMO−LUMO gap typically 1.3 to 1.6 eV calculated at the PBE0/def2-TZVPP/Th-ECP level; see Figure S3.

Investigation of all non-IPR structures was not feasible because there are over 5000 of them, and hence we studied only the 110 non-IPR isomers with two fused pentagons, which are supposed to be the most stable of the non-IPR isomers. The geometry optimizations were first carried out on the empty-cage tetra-anions of the 110 non-IPR isomers. The empty tetra-anionic non-IPR cages lie above the IPR C_{84}^{4-}-C_s(10) anion with an average E_r of ∼145 kJ/mol (Figure 3). The six

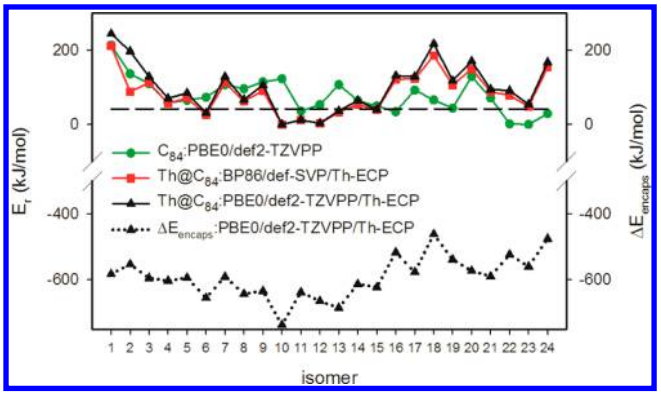

Figure 2. Comparison of relative electronic energy of empty C_{84} (green circles) and $Th@C_{84}$ (red squares and black triangles) IPR cages. Zero-energy level corresponds to the lowest C_{84} or $Th@C_{84}$ isomer, and dashed line illustrates ∼40 kJ/mol cutoff. The encapsulation energies ΔE_{encaps} are calculated as $\Delta E_{encaps} = E_{Th@C_{84}} - (E_{C_{84}} + E_{Th})$.

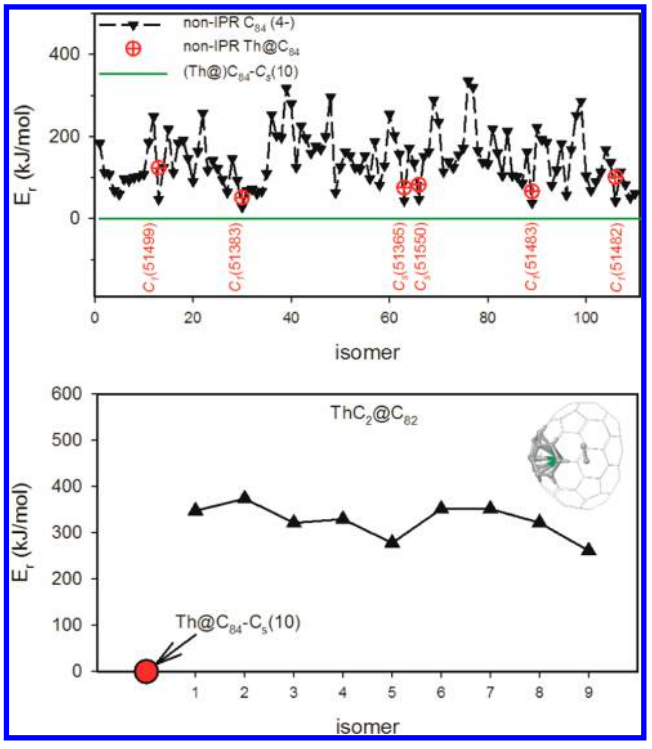

Figure 3. Top: Comparison of relative electronic energies of 110 non-IPR C_{84}^{4-} cages with C_{84}^{4-}-C_s(10) at the BP86/def-SVP/Th-ECP level. Selected non-IPR $Th@C_{84}$ are compared with $Th@C_{84}$-C_s(10) at the PBE0/def2-TZVPP/Th-ECP level. Bottom: Relative electronic energies of 9 $ThC_2@C_{82}$ isomers versus the lowest minimum $Th@C_{84}$-C_s(10) at PBE0/def2-TZVPP/Th-ECP level.

DOI: 10.1021/acs.jpca.7b00346
J. Phys. Chem. A 2017, 121, 3128−3135

energetically lowest non-IPR cages were selected for Th@C_{84} calculations and optimized at the PBE0/def2-TZVPP/Th-ECP level. They like about 50−100 kJ/mol above the lowest minimum Th@C_{84}-C_s(10). We note that the two previously experimentally observed non-IPR C_{84} cages, C_{84}-C_s(51365) and C_{84}-C_1(51383), (ref 82) are actually among the lowest non-IPR isomers. Their Th derivatives Th@C_{84}-C_s(51365) and Th@C_{84}-C_1(51383) lie ∼75 and ∼51 kJ/mol above the lowest minimum Th@C_{84}-C_s(10) isomer (green line in Figure 3.)

ThC_{84} stoichiometry may also correspond to a C_{82} fullerene cage encapsulating a carbide-like ThC_2 cluster.[1,83] Therefore, we minimized the nine IPR isomers of C_{82} with the ThC_2 cluster enclosed inside the cage. All tested ThC_2@C_{82} isomers were found to be higher in energy; see Figure 3. Thus the Th@C_{84}-C_s(10) should be the global minimum for ThC_{84} stoichiometry.

Notably, neither the empty C_{84}-C_s(10) cage nor its derivatives have been reported experimentally up to date. Thus the former observation of Th@C_{84} molecule[8] was likely also the first observation of the C_{84}-C_s(10) IPR isomer.

3.2. Lowest Energy Minimum, Th@C_{84}-C_S(10): Structure and Chemical Bonding. With the Th@C_{84}-C_s(10) identified as the lowest minimum structure for the Th@C_{84},we shall have a closer look at its electronic structure and properties. Figure 4 shows that Th is located approximately at a center of a

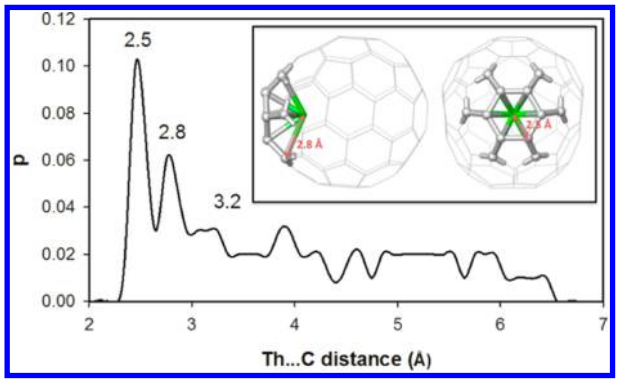

Figure 4. Radial distribution function calculated for all Th−C distances in the 24 IPR isomers of Th@C_{84} (Figure 1). Inset shows the Th@C_{84}-C_S(10) structure. All data are obtained at the PBE0/def2-TZVPP/Th-ECP level.

hexagon, with shortest Th−C contacts of 2.5 and 2.8 Å. The location of Th near the center of hexagon is a rather general principle among the 24 IPR isomers of Th@C_{84}, as seen from the molecular structures in Figure 1. The radial distribution function calculated from all of the Th−C distances in the 24 IPR Th@C_{84} isomers in Figure 4 shows two sharp maxima at 2.5 and 2.8 Å and also indicates a strong preference of Th to stay near the center of hexagon; see the inset of Figure 4.

Frontier canonical molecular orbitals of Th@C_{84}-C_S(10) are shown in Figure 5. We note that HOMO and HOMO−2 to HOMO−4 have Th-cage bonding character. HOMO−1 and LUMO+1 have antibonding Th−C character. The formal bond order between the cage and Th is thus (8/2−2/2) = 3, which may explain why the corresponding absorption edge in Th@C_{84} was found to be less reductive than in the reference $Th^{IV}(NO_3)_4$ material.

Th atom employs the 6d and 5f orbitals in bonding with cage, as can be seen in Figure 5. Atomic natural populations on Th thorium atom were evaluated as Th:$7s^{0.10}5f^{0.54}6d^{0.78}7p^{0.16}$, which points to polar covalent bonding between Th and cage and strong back-donation from cage to Th if $(Th^{4+})(C_{84}^{4-})$ system is considered. Note that 7p orbitals are slightly populated, which is probably given by the long-distance back-donation from more distant carbon atoms to Th 7p shell. Polar character of the Th-cage bonding is also supported by the NPA charge distribution; see Figure S4.

To assess further the character of the bonding between cage and Th atom in Th@C_{84}-C_s(10), we calculated the energy density and Laplacian of electron density (Figure 6) using Quantum Theory of Atoms in Molecules (QTAIM). The negative (red color) energy density $H(r)$ points to the localization of electrons between Th and nearby carbon atoms and hence covalent character of bonding between Th and the closest carbon atoms. The all-positive profile of Laplacian of energy density $\nabla^2\rho(r)$ (blue color) between Th and C atoms shows closed-shell bonding common in organometallics. The delocalization index, DI, defines the number of electrons that are shared between a pair of atoms and serves as an indicator of bond covalence. The DI indexes for the short Th−C contacts at 2.5 and 2.8 Å (Figure 4) are ∼0.3 (6×) and ∼0.2 (6×), summing up to three electrons. The total calculated DI for the 84 Th−C contacts is 4.2 electrons. This may point to involvement of the 6p shell in bonding with the cage. The bonding analysis overall points to Th in the oxidation state IV, with strong back-donation of one electron from the cage to Th atom.

3.3. UV−vis Absorption Spectra. The Th@C_{84} prepared by Akiyama et al. in the experimental study was characterized by its absorption spectrum.[8] Reproduction of the experimental spectrum by the theoretical one may provide further evidence of Th@C_{84}-C_s(10) being the compound observed in the experiment. However, rather limited literature exists on calculations of electronic absorption spectra in fullerenes and endohedral fullerenes.[54,55,58,84] Here we use the B3LYP functional with 6-31G* basis set on carbons that provided very good agreement between the theory and experiment in the past.[54−58] The basis set for Th with corresponding ECP[45] implemented under SDD name in Gaussian 09 code[38] was used.

The experimental electronic absorption spectra of Th@C_{84} in toluene exhibit five distinct bands at 1.35, 1.69, 1.94, 2.29, and 2.52 eV (Figure 7). The calculated spectrum for Th@C_{84}-C_s(10) reproduces the experimental one rather well. The theoretical "absorption threshold" is shifted to lower energies, and the 1.35 eV experimental bands appear split in two in the simulation. The bands at 1.69, 1.94, 2.29, and 2.22 eV are rather well reproduced; compare to lines 3, 4, 5, and 7 in Figure 7. This gives further evidence that the experimentally prepared system was the Th@C_{84}-C_s(10). Figure 7 further shows simplified interpretation of spectral bands by associating of individual lines in calculated spectrum with dominant orbital transitions. In future, magnetic circular dichroism spectra[54−56,58,84] might provide more reliable assignment of the electronic transitions than the absorption ones.

3.4. ^{13}C NMR Parameters in Th@C_{84}-C_s(10). To guide the future experimental work, the ^{13}C NMR chemical shifts were predicted for the lowest energy isomer Th@C_{84}-C_s(10) and for the five Th@C_{84} IPR isomers that lie within 40 kJ/mol from the lowest minimum. We used the two-component relativistic SO-ZORA at the PBE40/TZ2P level with the PBE0/def2-TZVPP/Th-ECP optimized structures that should provide

DOI: 10.1021/acs.jpca.7b00346
J. Phys. Chem. A 2017, 121, 3128−3135

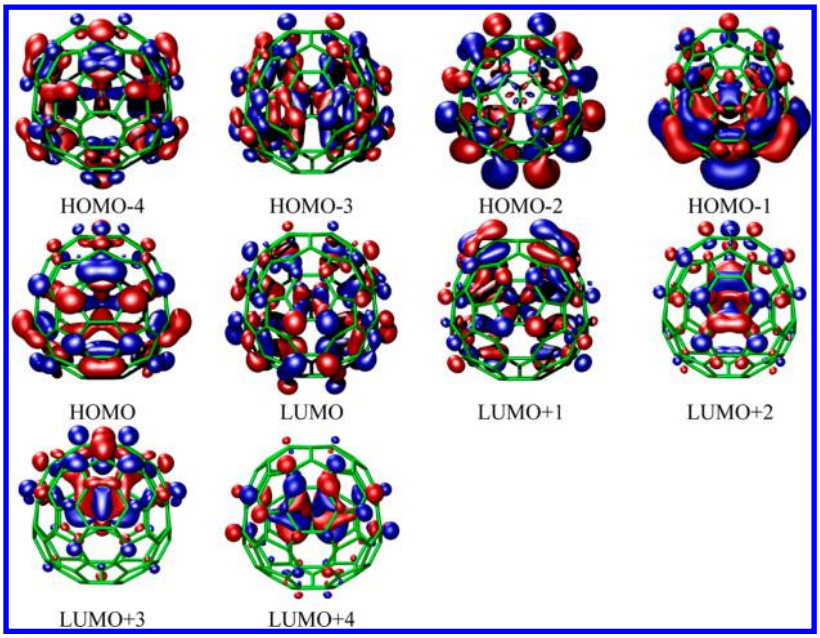

Figure 5. Selected canonical MOs of Th@C_{84}-C_S(10) calculated at the BP86/def-SVP/Th-ECP level. Isovalue of 0.025 eÅ^{-3} used.

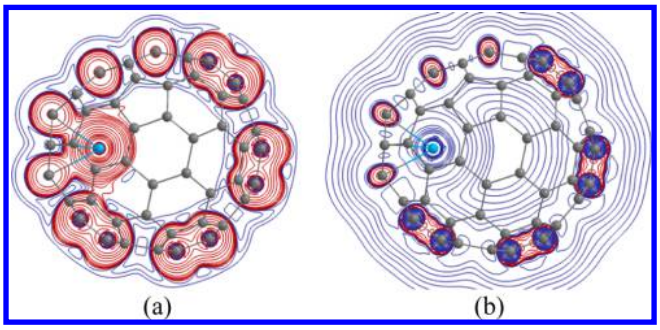

Figure 6. (a) Contour plot of energy density $H(r)$. (b) Contour plot of Laplacian of electron density $\nabla^2\rho(r)$.

rather accurate data for the light-atom chemical shifts in heavy-atom compounds.[71,76,79,83,85−89]

Because comparison to the experiment was not possible, we have briefly checked the dependence of the calculated ^{13}C chemical shifts on the optimized structure and basis set; see Figure S5. The difference between TZP and TZ2P basis set does not exceed 1 ppm, while the effect of differently optimized structures may cause changes up to 5 ppm.

The predicted ^{13}C NMR spectrum for Th@C_{84}-C_s(10) at the best level using SO-ZORA at PBE40/TZ2P level and PBE0/def2-TZVPP/Th-ECP structure is shown in Figure 8a. The ^{13}C spectrum lies in the range of 115−155 ppm, which belongs to standard ranges for C_{84} IPR isomers.[48] Figure 8b shows comparison of SO-ZORA and ZORA calculations and points to relatively small spin−orbit effects on ^{13}C chemical shifts, mostly deshielding.

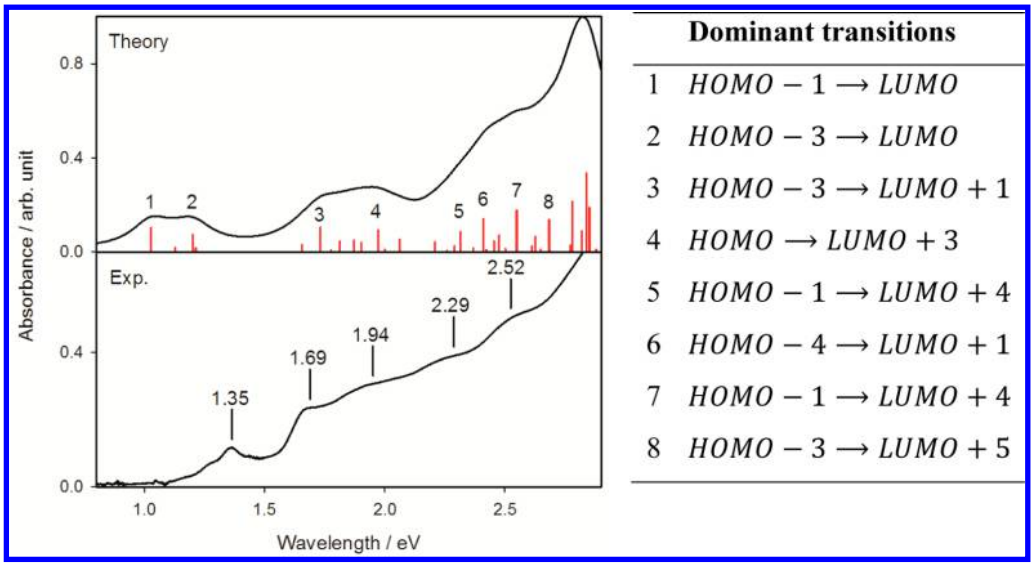

	Dominant transitions
1	$HOMO-1 \longrightarrow LUMO$
2	$HOMO-3 \longrightarrow LUMO$
3	$HOMO-3 \longrightarrow LUMO+1$
4	$HOMO \longrightarrow LUMO+3$
5	$HOMO-1 \longrightarrow LUMO+4$
6	$HOMO-4 \longrightarrow LUMO+1$
7	$HOMO-1 \longrightarrow LUMO+4$
8	$HOMO-3 \longrightarrow LUMO+5$

Figure 7. Experimental[8] and calculated (B3LYP/6-31G*/Th-ECP) electronic absorption spectra of Th@C_{84}-C_s(10). Table shows dominant transitions for selected lines of calculated line spectrum (labeled by numbers). Corresponding orbitals are depicted in Figure 5.

DOI: 10.1021/acs.jpca.7b00346
J. Phys. Chem. A 2017, 121, 3128−3135

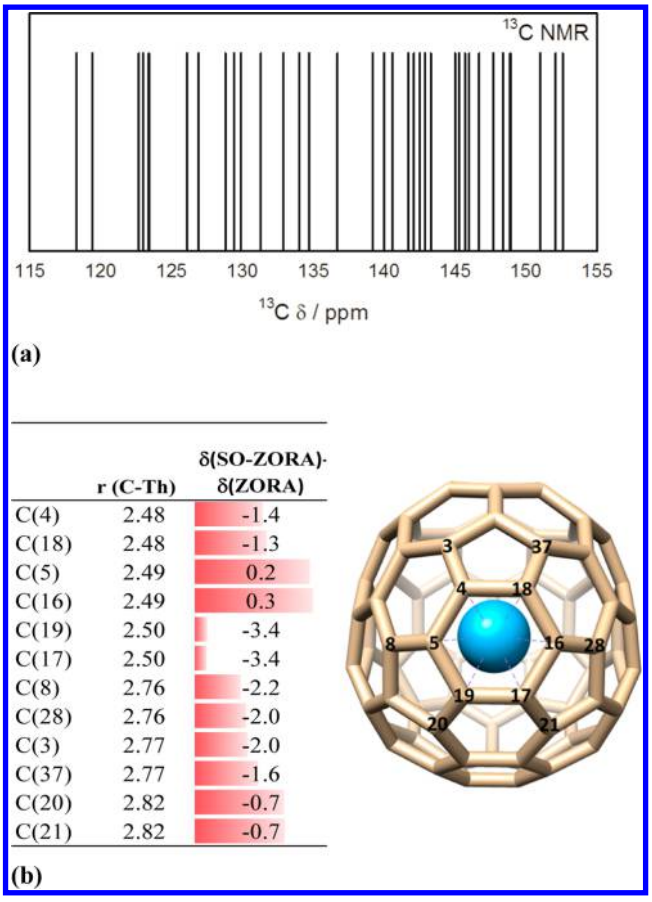

Figure 8. (a) NMR line spectrum for Th@C_{84}-C_s(10) simulated at the SO-ZORA PBE40/TZ2P//PBE0-def2-TZVPP/ECP level. Intensities are normalized. (b) SO effect on ^{13}C chemical shifts of selected carbons closest to Th atom (bottom). Full data are given in Table S1.

4. CONCLUSIONS

The only experimentally observed Th fullerene, Th@C_{84}, was studied theoretically to reveal its structure and molecular properties. The energy minimum was found to be a singlet state Th@C_{84}-C_s(10) IPR cage. The Th is located at a center of a hexagon, with shortest Th−C contacts of 2.5 and 2.8 Å. Bonding analysis revealed covalent-ionic character of the Th-cage bonding. According to the QTAIM analysis, Th shares nearly two electrons with the six closest carbons. Natural orbital occupation on Th atom, Th:$7s^{0.10}5f^{0.54}6d^{0.78}7p^{0.16}$, indicates polar bonding and back-donation of electrons from cage to the Th 5f and 6d orbitals, with involvement of 7p orbitals. Th can be considered in oxidation state IV, and one electron from the formally C_{84}^{4-} cage is back-donated to Th atom. Calculated UV−vis spectra of the Th@C_{84}-C_s(10) are consistent with the experimentally observed ones. All results support the original experimental work by Akiyama reporting for the first time the C_{84}-C_s(10) IPR cage. The predicted ^{13}C NMR chemical shifts of the lowest IPR isomers of Th@C_{84} may enhance future identification of Th@C_{84}.

■ ASSOCIATED CONTENT

Supporting Information

The Supporting Information is available free of charge on the ACS Publications website at DOI: 10.1021/acs.jpca.7b00346.

24 IPR isomers of C_{84} and their relative energies in kJ/mol; relative energies of the 24 isomers of C_{84} as obtained at various theoretical levels; HOMO−LUMO gap of 24 IPR Th@C_{84} isomers; the NPA charge distribution for empty C_{84}-Ca(10) cage and Th@C_{84}-C_a(10) isomer; comparison of calculated ^{13}C NMR shieldings in Th@C_{84}-C_s(10) (ppm) at various computational levels; calculated ^{13}C chemical shifts; and optimized structures of 24 Th@C_{84} IPR isomers, 6 selected non-IPR isomers, and 9 ThC_2@C_{82}isomers. (PDF)

■ AUTHOR INFORMATION

Corresponding Authors

*E-mail: kaminsky@uochb.cas.cz. Phone: (+420) 220 183 348. (J.K.)

*E-mail: straka@uochb.cas.cz. (M.S.)

ORCID

Jakub Kaminský: 0000-0001-6347-3022

Jan Vícha: 0000-0003-3698-8236

Notes

The authors declare no competing financial interest.

■ ACKNOWLEDGMENTS

We thank Kazuhiko Akiyama for the experimental UV−vis spectra of Th@C_{84}. Cina Foroutan-Nejad is acknowledged for the help with QTAIM calculations and James Avery for the help with the Fullerene program. The work was supported by the Czech Science Foundation (17-07091S to M.S. and 16-05935S to P.B.) and Program NPU I (LO1504 to J.V.). Computational resources were provided by the CESNET LM2015042 and the CERIT Scientific Cloud LM2015085, provided under the program "Projects of Large Research, Development, and Innovations Infrastructures".

■ REFERENCES

(1) Popov, A. A.; Yang, S.; Dunsch, L. Endohedral Fullerenes. *Chem. Rev.* **2013**, *113*, 5989−6113.

(2) Lu, X.; Bao, L.; Akasaka, T.; Nagase, S. Recent Progress in the Chemistry of Endohedral Metallofullerenes. *Chem. Commun.* **2014**, *50*, 14701−14715.

(3) Cong, H. L.; Yu, B.; Akasaka, T.; Lu, X. Endohedral Metallofullerenes: An Unconventional Core-Shell Coordination Union. *Coord. Chem. Rev.* **2013**, *257*, 2880−2898.

(4) Rivera-Nazario, D. M.; Pinzon, J. R.; Stevenson, S.; Echegoyen, L. A. Buckyball Maracas: Exploring the inside and Outside Properties of Endohedral Fullerenes. *J. Phys. Org. Chem.* **2013**, *26*, 194−205.

(5) Jin, P.; Tang, C.; Chen, Z. Carbon Atoms Trapped in Cages: Metal Carbide Clusterfullerenes. *Coord. Chem. Rev.* **2014**, *270*, 89−111.

(6) Wang, T.; Wang, C. Endohedral Metallofullerenes Based on Spherical I_h-C_{80} Cage: Molecular Structures and Paramagnetic Properties. *Acc. Chem. Res.* **2014**, *47*, 450−458.

(7) Garcia-Borras, M.; Osuna, S.; Luis, J. M.; Swart, M.; Sola, M. The Role of Aromaticity in Determining the Molecular Structure and Reactivity of (Endohedral Metallo)Fullerenes. *Chem. Soc. Rev.* **2014**, *43*, 5089−5105.

(8) Akiyama, K.; et al. Study of Metallofullerenes Encapsulating Actinides. *J. Nucl. Rad. Sci.* **2002**, *3*, 151−154.

(9) Guo, T.; Diener, M. D.; Chai, Y.; Alford, M. J.; Haufler, R. E.; McClure, S. M.; Ohno, T.; Weaver, J. H.; Scuseria, G. E.; Smalley, R. E. Uranium Stabilization of C_{28}: A Tetravalent Fullerene. *Science* **1992**, *257*, 1661−1664.

(10) Diener, M. D.; Smith, C. A.; Veirs, D. K. Anaerobic Preparation and Solvent-Free Separation of Uranium Endohedral Metallofullerenes. *Chem. Mater.* **1997**, *9*, 1773−1777.

DOI: 10.1021/acs.jpca.7b00346
J. Phys. Chem. A 2017, 121, 3128−3135

(11) Akiyama, K.; Saito, S.; Ando, T.; Iwasa, Y.; Kikuchi, K.; Kobayashi, M.; Saito, Y. Characterization of Actinide Metallofullerenes. *AIP Conf. Proc.* **2001**, *590*, 437−440.
(12) Akiyama, K.; et al. Isolation and Characterization of Light Actinide Metallofullerenes. *J. Am. Chem. Soc.* **2001**, *123*, 181−182.
(13) Akiyama, K.; Sueki, K.; Haba, H.; Tsukada, K.; Asai, M.; Yaita, T.; Nagame, Y.; Kikuchi, K.; Katada, M.; Nakahara, H. Production and Characterization of Actinide Metallofullerenes. *J. Radioanal. Nucl. Chem.* **2003**, *255*, 155−158.
(14) Dunk, P. W.; Kaiser, N. K.; Mulet-Gas, M.; Rodriguez-Fortea, A.; Poblet, J. M.; Shinohara, H.; Hendrickson, C. L.; Marshall, A. G.; Kroto, H. W. The Smallest Stable Fullerene, M@C_{28} (M = Ti, Zr, U): Stabilization and Growth from Carbon Vapor. *J. Am. Chem. Soc.* **2012**, *134*, 9380−9389.
(15) Dunk, P. W.; Mulet-Gas, M.; Nakanishi, Y.; Kaiser, N. K.; Rodriguez-Fortea, A.; Shinohara, H.; Poblet, J. M.; Marshall, A. G.; Kroto, H. W. Bottom-up Formation of Endohedral Mono-Metallofullerenes Is Directed by Charge Transfer. *Nat. Commun.* **2014**, *5*, 5844.
(16) Echegoyen, L.; Buck, D. New Endohedral Fullerenes Containing Uranium. In *227th ECS Meeting*, Chicago, IL, 2015, abstract 817.
(17) Fowler, P. W.; Austin, S. J.; Sandall, J. P. B. The Tetravalence of C28. *J. Chem. Soc., Perkin Trans. 2* **1993**, 795−797.
(18) Aihara, J.; Hosoya, H. Aromaticity of Multiply-Charged Fullerene Ions. *Bull. Chem. Soc. Jpn.* **1993**, *66*, 1955−1958.
(19) Jackson, K.; Kaxiras, E.; Pederson, M. R. Electronic States of Group-IV Endohedral Atoms in C_{28}. *Phys. Rev. B: Condens. Matter Mater. Phys.* **1993**, *48*, 17556−17561.
(20) Pitzer, R. M.; Zhao, K. Electronic Structure of C28, Pa@C28, and U@C_{28}. *J. Phys. Chem.* **1996**, *100*, 4798−4802.
(21) Dognon, J.-P.; Clavaguera, C.; Pyykko, P. A Predicted Organometallic Series Following a 32-Electron Principle: An@C_{28} (an = Th, Pa^{+}, U^{2+}, Pu^{4+}). *J. Am. Chem. Soc.* **2009**, *131*, 238−243.
(22) Ryzhkov, M. V.; Ivanovskii, A. L.; Delley, B. Electronic Structure of Endohedral Fullerenes An@C_{28} (An = Th - Md). *Comput. Theor. Chem.* **2012**, *985*, 46−52.
(23) Manna, D.; Ghanty, T. K. Prediction of a New Series of Thermodynamically Stable Actinide Encapsulated Fullerene Systems Fulfilling the 32-Electron Principle. *J. Phys. Chem. C* **2012**, *116*, 25630−25641.
(24) Ryzhkov, M. V.; Delley, B. Electronic Structure of Predicted Endohedral Fullerenes An@C_{40} (an = Th−Md). *Comput. Theor. Chem.* **2013**, *1013*, 70−77.
(25) Manna, D.; Ghanty, T. K. Enhancement in the Stability of 36-Atom Fullerene through Encapsulation of a Uranium Atom. *J. Phys. Chem. C* **2013**, *117*, 17859−17869.
(26) Manna, D.; Sirohiwal, A.; Ghanty, T. K. Pu@C_{24}: A New Example Satisfying the 32-Electron Principle. *J. Phys. Chem. C* **2014**, *118*, 7211−7221.
(27) Liu, X.; Li, L.; Liu, B.; Wang, D.; Zhao, Y.; Gao, X. Theoretical Study on the Ground State Structure of Uranofullerene U@C_{82}. *J. Phys. Chem. A* **2012**, *116*, 11651−5.
(28) Wu, X.; Lu, X. Dimetalloendofullerene U_2@C_{60} Has a U-U Multiple Bond Consisting of Sixfold One-Electron-Two-Center Bonds. *J. Am. Chem. Soc.* **2007**, *129*, 2171−2177.
(29) Infante, I.; Gagliardi, L.; Scuseria, G. E. Is Fullerene C_{60} Large Enough to Host a Multiply Bonded Dimetal? *J. Am. Chem. Soc.* **2008**, *130*, 7459−7465.
(30) Dai, X.; Meng, Y.; Xin, M.; Wang, F.; Fei, D.; Jin, M.; Wang, Z.; Zhang, R. Energetics and Electronic Properties of a Neutral Diuranium Molecule Encapsulated in C_{90} Fullerene. *Procedia Chem.* **2012**, *7*, 528−533.
(31) Dai, X.; Han, J.; Gao, Y.; Wang, Z. G. De Novo Design of an Endohedral Heteronuclear Dimetallofullerene (U-Gd)@C_{60} with Exceptional Structural and Electronic Properties. *ChemPhysChem* **2014**, *15*, 3871−3876.
(32) Han, J.; Dai, X.; Gao, Y.; Meng, Y.; Wang, Z. Defect-Induced Strong Localization of Uranium Dicarbide on the Graphene Surface. *Phys. Chem. Chem. Phys.* **2014**, *16*, 22784−22790.
(33) Foroutan-Nejad, C.; Vícha, J.; Marek, R.; Patzschke, M.; Straka, M. Unwilling U-U Bonding in U_2@C_{80}: Cage-Driven Metal-Metal Bonds in Di-Uranium Fullerenes. *Phys. Chem. Chem. Phys.* **2015**, *17*, 24182−24192.
(34) Gao, Y.; Wang, B.; Lei, Y.; Teo, B. K.; Wang, Z. Actinide-Embedded Gold Superatom Models: Electronic Structure, Spectroscopic Properties, and Applications in Surface-Enhanced Raman Scattering. *Nano Res.* **2016**, *9*, 622−632.
(35) Jiang, W.; Wang, Z. First-Principles Calculations of Magnetism in Nanoscale Carbon Materials Confining Metal with F Valence Electrons. *J. Cluster Sci.* **2016**, *27*, 845−860.
(36) Langeslay, R. R.; Fieser, M. E.; Ziller, J. W.; Furche, F.; Evans, W. J. Synthesis, Structure, and Reactivity of Crystalline Molecular Complexes of the $\{[C_5H_3(SiMe_3)_2]_3Th\}^{(1-)}$ Anion Containing Thorium in the Formal + 2 Oxidation State. *Chem. Sci.* **2015**, *6*, 517−521.
(37) *Turbomole V6.3 2011*, a Development of University of Karlsruhe and Forschungszentrum Karlsruhe Gmbhe 2007, 1989−2007.
(38) Frisch, M. J.; et al. *Gaussian 09*, revision D.01; Wallingford, CT, 2009.
(39) Štěpánek, P.; Bouř, P.; Straka, M. Assignment of the He@C_{84} Isomers in Experimental NMR Spectra Using Density Functional Calculations. *Chem. Phys. Lett.* **2010**, *500*, 54−58.
(40) Schwerdtfeger, P.; Wirz, L.; Avery, J. Program Fullerene: A Software Package for Constructing and Analyzing Structures of Regular Fullerenes. *J. Comput. Chem.* **2013**, *34*, 1508−1526.
(41) Schwerdtfeger, P.; Wirz, L. N.; Avery, J. The Topology of Fullerenes. *WIRE:Comp. Mol. Sci.* **2015**, *5*, 96−145.
(42) Adamo, C.; Barone, V. Toward Reliable Density Functional Methods without Adjustable Parameters: The Pbe0Model. *J. Chem. Phys.* **1999**, *110*, 6158−6170.
(43) Schafer, A.; Horn, H.; Ahlrichs, R. *J. Chem. Phys.* **1992**, *97*, 2571.
(44) Weigend, F.; Ahlrichs, R. Balanced Basis Sets of Split Valence, Triple Zeta Valence and Quadruple Zeta Valence Quality for H to Rn: Design and Assessment of Accuracy. *Phys. Chem. Chem. Phys.* **2005**, *7*, 3297−3305.
(45) Cao, X.; Dolg, M. *J. Mol. Struct.: THEOCHEM* **2004**, *673*, 203−209.
(46) Becke, A. D. Density-Functional Exchange-Energy Approximation with Correct Asymptotic Behavior. *Phys. Rev. A: At., Mol., Opt. Phys.* **1988**, *38*, 3098−3100.
(47) Perdew, J. P. *Phys. Rev. B: Condens. Matter Mater. Phys.* **1986**, *33*, 8822.
(48) Sun, G.; Kertesz, M. Isomer Identification for Fullerene C84 by 13C NMR Spectrum. A Density-Functional Theory Study. *J. Phys. Chem. A* **2001**, *105*, 5212−5220.
(49) Reed, A. E.; Curtiss, L. A.; Weinhold, F. Intermolecular Interactions from a Natural Bond Orbital, Donor-Acceptor Viewpoint. *Chem. Rev.* **1988**, *88*, 899−926.
(50) Reed, A. E.; Weinstock, R. B.; Weinhold, F. Natural Population Analysis. *J. Chem. Phys.* **1985**, *83*, 735−46.
(51) Humphrey, W.; Dalke, A.; Schulten, K. Vmd: Visual Molecular Dynamics. *J. Mol. Graphics* **1996**, *14*, 33−38.
(52) Bader, R. W. F. *Atoms in Molecules: A Quantum Theory*; Oxford University Press: Oxford, U.K., 1990.
(53) Keith, T. A. *AIMall*, version 13.05.06. http://aim.tkgristmill.com/.
(54) Fahleson, T.; Kauczor, J.; Norman, P.; Coriani, S. The Magnetic Circular Dichroism Spectrum of the C-60 Fullerene. *Mol. Phys.* **2013**, *111*, 1401−1404.
(55) Štepánek, P.; Straka, M.; Andrushchenko, V.; Bouř, P. Communication: Fullerene Resolution by the Magnetic Circular Dichroism. *J. Chem. Phys.* **2013**, *138*, 151103.
(56) Štěpánek, P.; Bouř, P. Computation of Magnetic Circular Dichroism by Sum over States Summations. *J. Comput. Chem.* **2013**, *34*, 1531−1539.
(57) Straka, M.; Štěpánek, P.; Coriani, S.; Vaara, J. Nuclear Spin Circular Dichroism in Fullerenes: A Computational Study. *Chem. Commun.* **2014**, *50*, 15228−15231.

DOI: 10.1021/acs.jpca.7b00346
J. Phys. Chem. A 2017, 121, 3128−3135

(58) Štěpánek, P.; Straka, M.; Šebestík, J.; Bouř, P. Magnetic Circular Dichroism of Chlorofullerenes: Experimental and Computational Study. *Chem. Phys. Lett.* **2016**, *647*, 117−121.
(59) Kupka, T.; Stachów, M.; Chełmecka, E.; Pasterny, K.; Stobińska, M.; Stobiński, L.; Kaminský, J. Efficient Modeling of NMR Parameters in Carbon Nanosystems. *J. Chem. Theory Comput.* **2013**, *9*, 4275−4286.
(60) Kupka, T.; Nieradka, M.; Kaminský, J.; Stobiński, L. Modeling ^{21}Ne NMR Parameters for Carbon Nanosystems. *Magn. Reson. Chem.* **2013**, *51*, 676−681.
(61) Kupka, T.; Stachów, M.; Stobinski, L.; Kaminský, J. ^{3}He NMR: From Free Gas to Its Encapsulation in Fullerene. *Magn. Reson. Chem.* **2013**, *51*, 463−468.
(62) Jankowska, M.; Kupka, T.; Stobiński, L.; Kaminský, J. DFT Studies on Armchair (5, 5) SWCNT Functionalization. Modification of Selected Structural and Spectroscopic Parameters Upon Two-Atom Molecule Attachment. *J. Mol. Graphics Modell.* **2015**, *55*, 105−114.
(63) Kupka, T.; Stachów, M.; Stobinski, L.; Kaminský, J. DFT Study of Zigzag (N, 0) Single-Walled Carbon Nanotubes: ^{13}C NMR Chemical Shifts. *J. Mol. Graphics Modell.* **2016**, *67*, 14−19.
(64) Kupka, T.; Stachów, M.; Stobinski, L.; Kaminský, J. Calculation of Raman Parameters of Real-Size Zigzag (N, 0) Single-Walled Carbon Nanotubes Using Finite-Size Models. *Phys. Chem. Chem. Phys.* **2016**, *18*, 25058−25069.
(65) Baerends, E. J.; et al. *ADF2014, SCM, Theoretical Chemistry*; Vrije Universiteit: Amsterdam, The Netherlands, 2014. http://www.scm.com/.
(66) Fonseca Guerra, C.; Snijders, J. G.; te Velde, G.; Baerends, E. J. Towards an Order-N DFT Method. *Theor. Chem. Acc.* **1998**, *99*, 391.
(67) te Velde, G.; Bickelhaupt, F. M.; van Gisbergen, S. J. A.; Fonseca Guerra, C.; Baerends, E. J.; Snijders, J. G.; Ziegler, T. Chemistry with ADF. *J. Comput. Chem.* **2001**, *22*, 931.
(68) van Lenthe, E.; Snijders, J. G.; Baerends, E. J. The Zero-Order Regular Approximation for Relativistic Effects: The Effect of Spin-Orbit Coupling in Closed Shell Molecules. *J. Chem. Phys.* **1996**, *105*, 6505−6516.
(69) van Lenthe, E.; Baerends, E. J.; Snijders, J. G. Relativistic Total-Energy Using Regular Approximations. *J. Chem. Phys.* **1994**, *101*, 9783−9792.
(70) van Lenthe, E.; Baerends, E. J.; Snijders, J. G. Relativistic Regular 2-Component Hamiltonians. *J. Chem. Phys.* **1993**, *99*, 4597−4610.
(71) Vícha, J.; Marek, R.; Straka, M. High-Frequency ^{13}C and ^{29}Si NMR Chemical Shifts in Diamagnetic Low-Valence Compounds of Tl(I) and Pb(II): Decisive Role of Relativistic Effects. *Inorg. Chem.* **2016**, *55*, 1770−1781.
(72) Vícha, J.; Foroutan-Nejad, C.; Pawlak, T.; Munzarova, M. L.; Straka, M.; Marek, R. Understanding the Electronic Factors Responsible for Ligand Spin-Orbit NMR Shielding in Transition-Metal Complexes. *J. Chem. Theory Comput.* **2015**, *11*, 1509−1517.
(73) Vícha, J.; Patzschke, M.; Marek, R. A Relativistic DFT Methodology for Calculating the Structures and NMR Chemical Shifts of Octahedral Platinum and Iridium Complexes. *Phys. Chem. Chem. Phys.* **2013**, *15*, 7740−7754.
(74) Hrobárik, P.; Hrobáriková, V.; Greif, A. H.; Kaupp, M. Giant Spin-Orbit Effects on NMR Shifts in Diamagnetic Actinide Complexes: Guiding the Search of Uranium(VI) Hydride Complexes in the Correct Spectral Range. *Angew. Chem., Int. Ed.* **2012**, *51*, 10884−10888.
(75) Greif, A. H.; Hrobárik, P.; Autschbach, J.; Kaupp, M. Giant Spin-Orbit Effects on 1H and 13C NMR Shifts for Uranium(VI) Complexes Revisited: Role of the Exchange-Correlation Response Kernel, Bonding Analyses, and New Predictions. *Phys. Chem. Chem. Phys.* **2016**, *18*, 30462−30474.
(76) Vícha, J.; Novotný, J.; Straka, M.; Repisky, M.; Ruud, K.; Komorovsky, S.; Marek, R. Structure, Solvent, and Relativistic Effects on the NMR Chemical Shifts in Square-Planar Transition-Metal Complexes: Assessment of DFT Approaches. *Phys. Chem. Chem. Phys.* **2015**, *17*, 24944−24955.
(77) van Lenthe, E.; Baerends, E. J. Optimized Slater-Type Basis Sets for the Elements 1−118. *J. Comput. Chem.* **2003**, *24*, 1142−1156.
(78) Chong, P. C.; van Lenthe, E.; van Gisbergen, S. J. A.; Baerends, E. J. Even-Tempered Slater-Type Orbitals Revisited: From Hydrogen to Krypton. *J. Comput. Chem.* **2004**, *25*, 1030−1036.
(79) Kaminský, J.; Buděšinský, M.; Taubert, S.; Bouř, P.; Straka, M. Fullerene C-70 Characterization by C-13 NMR and the Importance of the Solvent and Dynamics in Spectral Simulations. *Phys. Chem. Chem. Phys.* **2013**, *15*, 9223−9230.
(80) Avent, A. G.; Dubois, D.; Penicaud, A.; Taylor, R. The Minor Isomers and IR Spectrum of [84]fullerene. *J. Chem. Soc., Perkin Trans. 2* **1997**, *2*, 1907.
(81) Fowler, P. W.; Manolopoulos, D. E. *An Atlas of Fullerenes*; Oxford University Press: Oxford, U.K., 1995.
(82) Fuhrer, T. J.; Lambert, A. M. Isolated Pentagon Rule Violating Endohedral Metallofullerenes Explained Using the Huckel Rule: A Statistical Mechanical Study of the C_{84} Isomeric Set. *J. Comput. Chem.* **2015**, *36*, 146−50.
(83) Taubert, S.; Straka, M.; Pennanen, T. O.; Sundholm, D.; Vaara, J. Dynamics and Magnetic Resonance Properties of Sc_3C_2@C_{80} and Its Monoanion. *Phys. Chem. Chem. Phys.* **2008**, *10*, 7158−7168.
(84) Yamada, M.; Slanina, Z.; Mizorogi, N.; Muranaka, A.; Maeda, Y.; Nagase, S.; Akasaka, T.; Kobayashi, N. Application of MCD Spectroscopy and TD-DFT to Endohedral Metallofullerenes for Characterization of Their Electronic Transitions. *Phys. Chem. Chem. Phys.* **2013**, *15*, 3593−3601.
(85) Vícha, J.; Foroutan-Nejad, C.; Pawlak, T.; Munzarová, M. L.; Straka, M.; Marek, R. Understanding the Electronic Factors Responsible for Ligand Spin-Orbit NMR Shielding in Transition-Metal Complexes. *J. Chem. Theory Comput.* **2015**, *11*, 1509−1517.
(86) Vícha, J.; Straka, M.; Munzarová, M. L.; Marek, R. Mechanism of Spin-Orbit Effects on the Ligand NMR Chemical Shift in Transition-Metal Complexes: Linking NMR to EPR. *J. Chem. Theory Comput.* **2014**, *10*, 1489−1499.
(87) Standara, S.; Kulhánek, P.; Marek, R.; Straka, M. ^{129}Xe NMR Chemical Shift in Xe@C_{60} Calculated at Experimental Conditions: Essential Role of the Relativity, Dynamics, and Explicit Solvent. *J. Comput. Chem.* **2013**, *34*, 1890−1898.
(88) Hyvärinen, M.; Vaara, J.; Goldammer, A.; Kutzky, B.; Hegetschweiler, K.; Kaupp, M.; Straka, M. Characteristic Spin-Orbit Induced H-1(CH2) Chemical Shifts Upon Deprotonation of Group 9 Polyamine Aqua and Alcohol Complexes. *J. Am. Chem. Soc.* **2009**, *131*, 11909−11918.
(89) Straka, M.; Lantto, P.; Vaara, J. Toward Calculations of the ^{129}Xe Chemical Shift in Xe@C_{60} at Experimental Conditions: Relativity, Correlation, and Dynamics. *J. Phys. Chem. A* **2008**, *112*, 2658−2668.

DOI: 10.1021/acs.jpca.7b00346
J. Phys. Chem. A 2017, 121, 3128−3135